Available online at www.sciencedirect.com
ScienceDirect
Applied Catalysis B: Environmental 82 (2008) 37–49
APPLIED CATALYSIS B: ENVIRONMENTAL
www.elsevier.com/locate/apcatb

Photocatalytic degradation of 4-chlorophenol: A kinetic study

María L. Satuf, Rodolfo J. Brandi, Alberto E. Cassano, Orlando M. Alfano *

INTEC, Universidad Nacional del Litoral and CONICET, Güemes 3450, S3000GLM, Santa Fe, Argentina

Received 4 September 2007; received in revised form 28 December 2007; accepted 7 January 2008
Available online 15 January 2008

Abstract

A kinetic study of the photocatalytic degradation of 4-chlorophenol employing titanium dioxide is presented. Experiments were carried out in a cylindrical slurry reactor irradiated by UV lamps. The aromatic reaction intermediates were identified and quantified. Intrinsic expressions to represent the kinetics of 4-chlorophenol and the main intermediates, 4-chlorocatechol and hydroquinone, were derived from a proposed reaction scheme. These expressions include explicitly the effect of photon absorption on the reaction rate. The modeling of the radiation field in the reactor was accomplished by solving the radiative transfer equation with the discrete ordinate method. Experimental runs were performed by varying the catalyst concentration, the incident radiation, and the reactor length. The parameters of the kinetic model were estimated from the experiments by applying a non-linear regression procedure. Good agreement was obtained between model predictions and experimental data, with a root mean square error of 14.4%.

Keywords: 4-Chlorophenol; Photocatalysis; Photon absorption; Kinetics

1. Introduction

Heterogeneous photocatalysis employing titanium dioxide (TiO_2) has been successfully applied to degrade hazardous compounds from air and water [1–5]. One of the main advantages of this oxidation process is that it can provide the mineralization of a wide range of pollutants under mild reaction conditions. Furthermore, it is possible to employ solar radiation to activate the process.

Chlorophenols represent an important group of water pollutants that can be degraded by photocatalysis. Due to their toxicity and low biodegradability, they are considered as priority pollutants [6]. Chlorophenols are employed in numerous industrial processes and, in particular, 4-chlorophenol (4-CP) is involved in the synthesis of many pesticides, pharmaceuticals, and dyes. The kinetics of the photocatalytic degradation of 4-CP has been extensively studied [7–14]. However, most researchers have employed Langmuir–Hinshelwood type of kinetic expressions to represent the reaction rate, where model parameters depend on experimental conditions (radiation flux, catalyst concentration, reactor configuration, etc.). Therefore, these kinetic equations are not applicable to different reactors or under different operating conditions. Only intrinsic kinetic data, obtained from models that involve the solution of the mass balances of the reacting species and the evaluation of the radiation field in the employed reactor, can be used to design, optimize or scale-up photocatalytic reactors.

Several approaches to evaluate the radiation field in slurry reactors have been reported, involving actinometric and radiometric measurements, and the application of mathematical models to obtain the rate of photon absorption in the reaction space [15–22].

In the present work, we propose intrinsic kinetic expressions for the photocatalytic degradation of 4-CP, as well as equations to represent the formation and disappearance of the main intermediate products: 4-chlorocatechol (4-CC) and hydroquinone (HQ). The study was carried out in a slurry photoreactor, employing artificial UV light as the source of energy and TiO_2 as catalyst. The kinetic equations are based on mechanistic reaction steps and include the modeling of radiation absorption and scattering effects. The radiation field was evaluated by applying the radiative transfer equation (RTE) to the heterogeneous system.

* Corresponding author. Fax: +54 342 4511087.
E-mail address: alfano@intec.unl.edu.ar (O.M. Alfano).

0926-3373/$ – see front matter © 2008 Elsevier B.V. All rights reserved.
doi:10.1016/j.apcatb.2008.01.003

Nomenclature

a_v	catalytic surface area per unit suspension volume (cm^{-1})
4-CC	4-chlorocatechol
4-CP	4-chlorophenol
C	molar concentration in the suspension bulk (mol cm^{-3})
C_m	catalyst mass concentration (g cm^{-3})
e^a	local volumetric rate of photon absorption (Einstein cm^{-3} s^{-1})
g	asymmetry factor
HQ	hydroquinone
I	radiation intensity (Einstein cm^{-2} sr^{-1} s^{-1})
K	equilibrium adsorption constant (cm^3 mol^{-1})
k	kinetic constant (cm^2 mol^{-1} s^{-1})
L_R	reactor length (cm)
n	refractive index
p	phase function
Q_L	radiation level (%)
RMSE	root mean square error (%)
r	superficial reaction rate (mol cm^{-2} s^{-1})
r_{gs}	superficial rate of electron–hole generation (mol cm^{-2} s^{-1})
S_g	catalyst specific surface area (cm^2 g^{-1})
TOC	total organic carbon (mol cm^{-3})
t	time (s)
V	volume (cm^3)
X_i, X_j	secondary organic intermediates
x	axial coordinate (cm)
x	position vector (cm)
Y_l	inorganic radicals and species

Greek letters

α_i, α'_i	kinetic parameter
β	volumetric extinction coefficient (cm^{-1})
β^*	specific extinction coefficient (cm^2 g^{-1})
ε	hold-up
γ	optical thickness
κ	volumetric absorption coefficient (cm^{-1})
κ^*	specific absorption coefficient (cm^2 g^{-1})
μ	direction cosine of the ray for which the RTE is written
μ'	direction cosine of an arbitrary ray before scattering
μ_0	cosine of the angle between the direction of the incident and the scattered rays
μ_c	cosine of the critical angle θ_c
ν	stoichiometric coefficient
$\bar{\phi}$	wavelength averaged primary quantum yield (mol $Einstein^{-1}$)
σ	volumetric scattering coefficient (cm^{-1})
σ^*	specific scattering coefficient (cm^2 g^{-1})
Γ_W	global reflection coefficient of the reactor windows
θ	spherical coordinate (rad)
θ_c	critical angle (rad)

Subscripts

ads	adsorbed on the catalyst surface
A_R	catalytic reaction area
4-CC	4-chlorocatechol
4-CP	4-chlorophenol
HQ	hydroquinone
HG	Henyey and Greenstein
L_R	relative to the reactor window at $x = L_R$
R	reactor
T	total
Tk	tank
0	initial condition; also, relative to the reactor window at $x = 0$
λ	dependence on wavelength

Special symbol

[]	concentration on the catalyst surface (mol cm^{-2})

2. Experimental

2.1. Chemicals

4-Chlorophenol (4-CP, >99%), obtained from Aldrich, was employed as the model pollutant. Hydroquinone (HQ, >99.0%) and benzoquinone (BQ, >98.0%), both from Fluka, and 4-chlorocatechol (4-CC, 97%) from Aldrich, were used to identify and quantify the intermediate products. All chemicals were employed as received without further purification. Reagent grade perchloric acid was used to adjust the pH of the reacting mixture. TiO_2 powder (99.8% anatase, specific surface area 9.6 m^2 g^{-1}) was obtained from Aldrich. All solutions were prepared with deionized and doubly distilled water.

2.2. Experimental device

The photocatalytic degradation of 4-CP was carried out in a cylindrical reactor made of stainless steel, with an inner wall of Teflon, and two circular, borosilicate glass windows. The reactor has a special mechanism of mobile windows that allows one to change, in a precise way, the reactor length L_R (Figs. 1 and 2). This feature gives us the possibility to study the influence of the optical thickness on kinetic parameters over a wide range of values, as it will be explained in Section 2.4.

Radiant energy was supplied by two sets of four lamps each (TL 4W/08 Black Light UVA lamps from Philips) placed vertically inside metal boxes on both sides of the reactor. The wavelength emission range of the lamps was 300–400 nm, with a peak near 350 nm. The radiation flux that reached the reactor windows was experimentally measured by ferrioxalate actinometry [23]. Optical neutral filters were used to carry out experiments at different irradiation levels. Also, ground glass plates were located between the lamps and the reactor to produce diffuse inlet radiation.

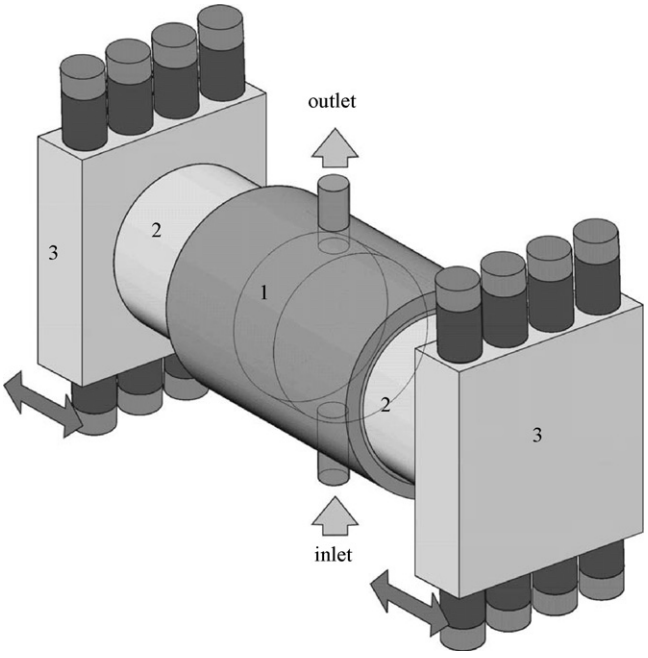

Fig. 1. Schematic representation of the photocatalytic reactor. 1: reactor; 2: mobile windows system; 3: radiation emitting system.

The reactor was operated in a recirculation batch mode, as shown in Fig. 3. The storing tank was fitted with a sampling valve, a gas inlet for oxygen supply, and a water-circulating jacket to ensure isothermal conditions during the reaction time. A magnetic drive gear pump (Micropump®) was employed to recirculate the suspension in the system.

The dimensions and main characteristics of the experimental set up are summarized in Table 1.

2.3. Procedure

The reacting suspension comprised a defined amount of 4-CP and TiO_2 dispersed in a total volume (V_T) of 1000 cm^3.

Table 1
Experimental set up

Component	Parameter	Value
Reactor	Inner diameter	8.6 cm
	Length (min–max)	(0.5–5.0) cm
	Reactor volume (min–max)	(29–290) cm^3
	Total volume	1000 cm^3
Lamps	Nominal power	4 W (each)
	Emission range	300–400 nm
	Radiation flux (100%)[a]	7.55×10^{-9} Einstein cm^{-2} s^{-1}
	Diameter	1.6 cm
	Arc length	13.6 cm
Pump	Flow rate	100 cm^3 s^{-1}
Thermostatic bath	Temperature[b]	293 K

Dimensions and main characteristics.
[a] At the reactor windows.
[b] Measured in the tank.

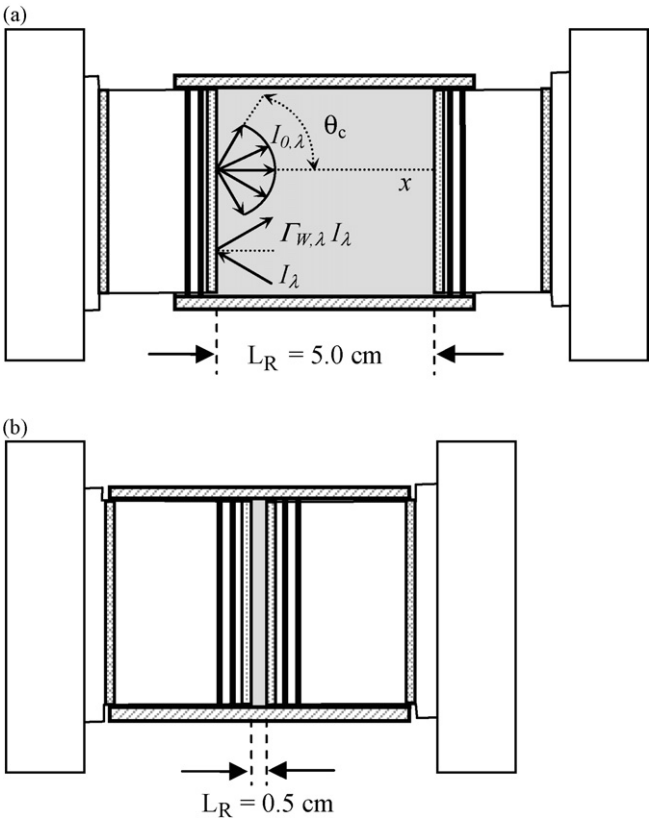

Fig. 2. Mobile windows mechanism, including the coordinate system for the radiation model: (a) maximum length; (b) minimum length.

Previous experiments [24] showed that the 4-CP removal efficiency was improved under acidic conditions. Consequently, the pH of the mixture was adjusted to 2.5 with perchloric acid. The suspension was sonicated during 30 min and then added to the tank. The reacting mixture, circulating at a flow rate of 100 cm^3 s^{-1}, was saturated with pure oxygen by intense bubbling for 45 min. The pump flow rate provided good mixing conditions, low conversion per pass in the reactor, and uniform concentration of the catalyst throughout the system. During this time interval, the UV lamps were turned on in order to stabilize the radiation emission. Shutters located between the lamps and each reactor window prevented radiation to arrive at the reactor. Then, the initial sample was taken ($t = 0$). Immediately, the shutters were removed and the experimental run started. Each run lasted 8 h and samples were obtained from the tank every hour. The temperature throughout the experiments was kept at 293 K, and the system was maintained under overpressure of oxygen to guarantee the renewal of the oxygen consumed by the photocatalytic reaction. All samples were centrifuged and filtered with a 0.02 μm syringe filter (Anotop 25) to remove the catalyst particles before analyses.

A control experiment was carried out to evaluate direct photolysis. The experiment was conducted following the procedure indicated above but without the addition of TiO_2. No detectable changes occurred in the concentration of 4-CP after 10 h of irradiation.

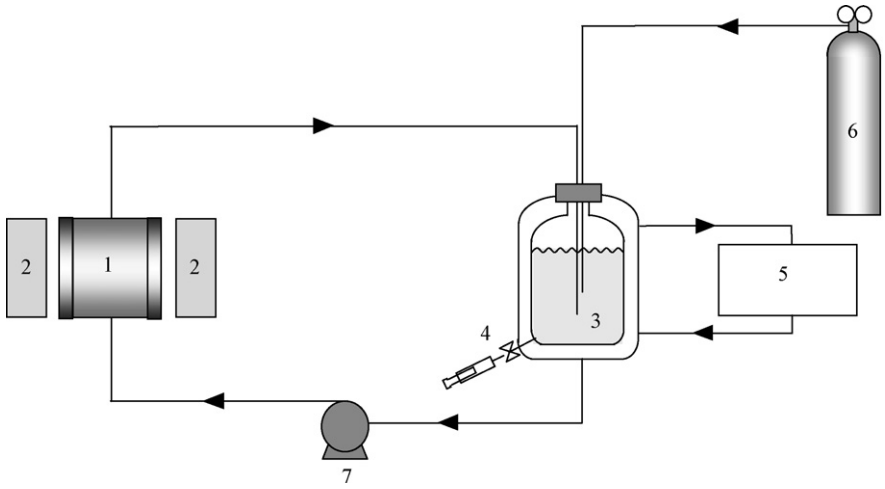

Fig. 3. Schematic representation of the experimental set up. 1: reactor; 2: radiation emitting system; 3: tank; 4: sampling valve; 5: thermostatic bath; 6: oxygen supply; 7: pump.

2.4. Experimental conditions

Experiments were performed by varying the catalyst concentration (C_m), the level of incident radiation (Q_L), and the reactor length (L_R). Details of the operating conditions of the experiments are reported in Table 2.

The Influence of the optical thickness on kinetic parameters constitutes a key aspect in the modeling of slurry photocatalytic reactors. The optical thickness γ_λ can be defined as a new variable of the system as

$$\gamma_\lambda = \beta_\lambda L_R \quad (1)$$

where β_λ is the volumetric extinction coefficient ($\beta_\lambda = \beta^*_\lambda C_m$). The optical thickness can be modified by changing the catalyst concentration, with the resulting modification of β_λ, or by changing the reactor length. Note that γ_λ depends on the radiation wavelength through β_λ. Considering the wavelength corresponding to the maximum emission of the lamps, $\lambda = 350$ nm, the values of γ_λ in our experiments ranged from 0.37 (for $C_m = 0.05 \times 10^{-3}$ g cm^{-3} and $L_R =$ 0.5 cm) to 74 (for $C_m = 1.0 \times 10^{-3}$ g cm^{-3} and $L_R = 5.0$ cm), i.e. γ_λ varies 2 orders of magnitude. This procedure allows us to work under very different conditions of irradiation in the reaction space: (i) at low γ_λ, the reactor is uniformly irradiated; (ii) at high γ_λ, radiation is almost completely absorbed near the windows and the center of the reactor remains nearly dark.

Table 2
Operating conditions of the experiments

Variable	Values
Catalyst concentration (C_m)	0.05, 0.1, 0.5, and 1.0×10^{-3} g cm^{-3}
Level of incident radiation (Q_L)	30, 67, and 100%
Reactor length (L_R)	0.5, 1.0, and 5.0 cm
Initial concentration of 4-CP	1.5×10^{-7} mol cm^{-3}
Initial pH	2.5

2.5. Analysis

The concentration of 4-CP and its reaction intermediates were measured by HPLC using a Waters chromatograph equipped with a LC-18 Supelcosil reversed phase column (Supelco). The species present in the sample solutions were identified by comparing the retention time of the detected peaks with the retention time of standards. The eluent was a ternary mixture of water (containing 1%, v/v, acetic acid), methanol, and acetonitrile (60:30:10), pumped at a rate of 1 cm^3 min^{-1}. UV detection of 4-CP and the aromatic intermediates was performed at 280 nm, except for BQ, whose concentration was measured at 254 nm.

The photocatalytic degradation of 4-CP involves the cleavage of the aryl–Cl bond, releasing inorganic chloride to the reacting medium. Consequently, chloride measurements were made to follow the advance of the reaction. Chloride was quantified using a Dionex ion chromatograph provided with an anionic analytical column (Dionex IonPack AS4A-SC), a suppressor cell and a conductivity detector. The mineralization of the pollutant was assessed by total organic carbon (TOC) analysis, employing a Shimadzu TOC-5000 A analyzer. UV absorption spectra of the samples were acquired in a Cary 100 Bio UV–vis spectrophotometer.

3. Theoretical

3.1. Mass balances

The mass balances of the model pollutant and the intermediate products were solved in order to obtain the theoretical evolution of each species. To accomplish this, a number of assumptions were made: (i) there is a differential conversion per pass in the reactor, (ii) the system is perfectly stirred, (iii) there are no mass transport limitations, (iv) the chemical reaction occurs only at the solid–liquid interface [25,26], and (v) direct photolysis is neglected. As a result, the mass balance for a species i in the system takes the following

form [16]:

$$\varepsilon_L \left.\frac{dC_i(t)}{dt}\right|_{Tk} = \frac{V_R}{V_T} a_v \nu_i \langle r(\mathbf{x},t)\rangle_{A_R} \quad (2)$$

where ε_L is the liquid hold-up ($\varepsilon_L \cong 1$), C_i is the molar concentration of i, t denotes reaction time, Tk refers to the tank, V_R is the reactor volume, V_T is the total system volume, a_v denotes the catalytic surface area per unit suspension volume, ν_i is the stoichiometric coefficient, and $\langle r(\mathbf{x},t)\rangle_{A_R}$ is the superficial reaction rate averaged over the catalytic reaction area, A_R. The value of a_v is computed from the product of the catalyst specific surface area (S_g) and the catalyst loading (C_m).

The primary photocatalytic oxidation products of 4-CP are 4-CC, HQ, and BQ [12]. Under the experimental conditions employed in our work, at pH 2.5, 4-CC was the most abundant intermediate, followed by HQ. The concentration of BQ never reached significant levels, therefore it was not considered in the kinetic model. As will be described in Section 3.2, we propose a parallel degradation mechanism of 4-CP to give 4-CC and HQ.

Then, the mass balances for 4-CP, 4-CC and HQ, with the corresponding initial conditions, are

$$\varepsilon_L \left.\frac{dC_{4\text{-CP}}(t)}{dt}\right|_{Tk} = -\frac{V_R}{V_T} a_v \{\langle r_{4\text{-CP},1}(\mathbf{x},t)\rangle_{A_R} + \langle r_{4\text{-CP},2}(\mathbf{x},t)\rangle_{A_R}\}$$
$$C_{4\text{-CP}}(t=0) = C_{4\text{-CP},0} \quad (3)$$

$$\varepsilon_L \left.\frac{dC_{4\text{-CC}}(t)}{dt}\right|_{Tk} = \frac{V_R}{V_T} a_v \{\langle r_{4\text{-CP},1}(\mathbf{x},t)\rangle_{A_R} - \langle r_{4\text{-CC}}(\mathbf{x},t)\rangle_{A_R}\}$$
$$C_{4\text{-CC}}(t=0) = 0 \quad (4)$$

$$\varepsilon_L \left.\frac{dC_{HQ}(t)}{dt}\right|_{Tk} = \frac{V_R}{V_T} a_v \{\langle r_{4\text{-CP},2}(\mathbf{x},t)\rangle_{A_R} - \langle r_{HQ}(\mathbf{x},t)\rangle_{A_R}\}$$
$$C_{HQ}(t=0) = 0 \quad (5)$$

$r_{4\text{-CP},1}$ represents the degradation rate of 4-CP to give 4-CC, whereas $r_{4\text{-CP},2}$ is the rate that leads to the formation of HQ. $r_{4\text{-CC}}$ and r_{HQ} denote the degradation rates of 4-CC and HQ, respectively (Fig. 4).

3.2. Kinetic model

The kinetic model proposed for the photocatalytic degradation of 4-CP is based on the reaction scheme summarized in Table 3 [2,27]. The absorption of UV radiation by TiO_2 promotes an electron from the valence band of the semiconductor into the conduction band, leaving a positively charged hole in the valence band (S1). The photogenerated electron–hole pair migrates to the surface of the catalyst particle and reacts with surface species. The electrons and holes have to be trapped to prevent recombination and the resulting loss of energy as heat (S2). Electrons can be trapped by molecular oxygen, generating the superoxide radical anion (S3). Holes can be trapped by water molecules or hydroxyl ions adsorbed at the catalyst surface, leading to the formation of hydroxyl radicals, $^{\bullet}OH$ (S4). Although photogenerated holes can attack the pollutant directly, we consider the indirect

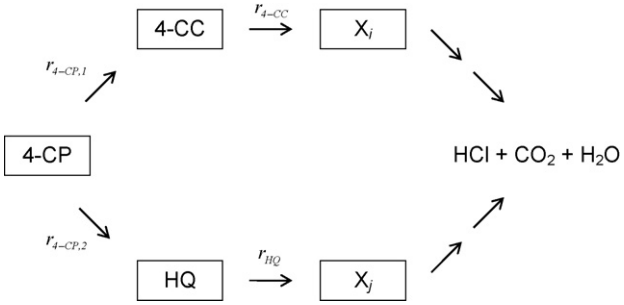

Fig. 4. Reaction network of the photocatalytic degradation of 4-CP.

pathway (via $^{\bullet}OH$) as the dominant reaction route for the degradation of 4-CP (S5, S6) [10,12,28]. The primary organic intermediates of the reaction, i.e. 4-CC and HQ, can be further degraded by oxidation with $^{\bullet}OH$ (S7, S8). In Table 3, X_i and X_j represent the secondary organic intermediates of the reaction, whereas Y_l represents inorganic radicals and species that compete with the organic substrate for $^{\bullet}OH$ (S9) [27]. Fig. 5 shows the main reaction path proposed for the formation of the primary intermediates of 4-CP in acidic medium [10,12].

The kinetic model assumes that photocatalytic reactions occur at the surface of the catalyst particles among adsorbed species [26], and that dynamic equilibrium is achieved between bulk and adsorbed concentrations of water, oxygen, organic compounds, and inorganic species [27,29]. Molecular oxygen and organic compounds are considered to adsorb on different sites of the TiO_2 particle [2,30]. On the other hand, since adsorption sites for the organics are assumed to be the same, a competitive adsorption mechanism for 4-CP and its main intermediates is postulated. Consequently, the following equations can be written:

$$[\text{4-CP}_{ads}] = K_{4\text{-CP}}[\text{site}_{4\text{-CP}}]C_{4\text{-CP}} \quad (6)$$

$$[\text{4-CC}_{ads}] = K_{4\text{-CC}}[\text{site}_{4\text{-CP}}]C_{4\text{-CC}} \quad (7)$$

Table 3
Reaction scheme for the photocatalytic degradation of 4-CP

Step	Reaction	Rate	
Activation	$TiO_2 + h\upsilon \rightarrow TiO_2 + e^- + h^+$	r_{gs}	S1
Recombination	$e^- + h^- \rightarrow$ heat	$k_2[e^-][h^+]$	S2
Electron trapping	$e^- + O_{2,ads} \rightarrow {}^{\bullet}O_2^-$	$k_3[e^-][O_{2,ads}]$	S3
Hole trapping	$h^+ + H_2O_{ads} \rightarrow {}^{\bullet}OH + H^+$ $h^+ + OH_{ads}{}^- \rightarrow {}^{\bullet}OH$	$k_4[h^+][H_2O_{ads}]$	S4
Hydroxyl attack	$\text{4-CP}_{ads} + {}^{\bullet}OH \rightarrow$ 4-CC $\text{4-CP}_{ads} + {}^{\bullet}OH \rightarrow$ HQ $\text{4-CC}_{ads} + {}^{\bullet}OH \rightarrow X_i$ $HQ_{ads} + {}^{\bullet}OH \rightarrow X_j$ $Y_{l,ads} + {}^{\bullet}OH \rightarrow Y_m$	$k_5[{}^{\bullet}OH][\text{4-CP}_{ads}]$ $k_6[{}^{\bullet}OH][\text{4-CP}_{ads}]$ $k_7[{}^{\bullet}OH][\text{4-CC}_{ads}]$ $k_8[{}^{\bullet}OH][HQ_{ads}]$ $k_1''[{}^{\bullet}OH][Y_{l,ads}]$	S5 S6 S7 S8 S9
Adsorption	$\text{Site}_{O_2} + O_2 \leftrightarrow O_{2,ads}$ $\text{Site}_{H_2O} + H_2O \leftrightarrow H_2O_{ads}$ $\text{Site}_{H_2O} + H_2O \leftrightarrow OH_{ads}{}^- + H^+$ $\text{Site}_{4\text{-CP}} + \text{4-CP} \leftrightarrow \text{4-CP}_{ads}$ $\text{Site}_{4\text{-CP}} + \text{4-CC} \leftrightarrow \text{4-CC}_{ads}$ $\text{Site}_{4\text{-CP}} + HQ \leftrightarrow HQ_{ads}$ $\text{Site}_{Y_l} + Y_l \leftrightarrow Y_{l,ads}$		

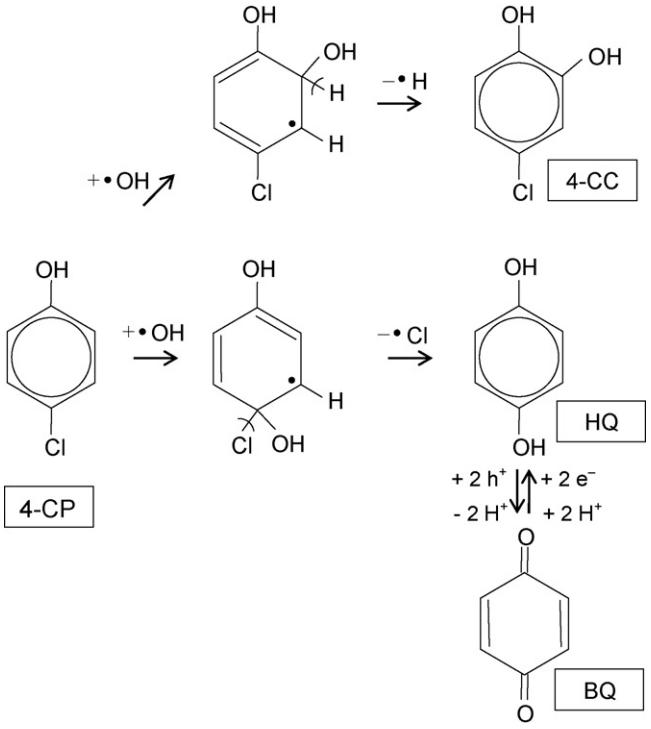

Fig. 5. Reaction pathway suggested for the formation of the primary aromatic intermediates of 4-chlorophenol in acidic medium.

$$[\mathrm{HQ_{ads}}] = K_{\mathrm{HQ}}[\mathrm{site_{4\text{-}CP}}]C_{\mathrm{HQ}} \tag{8}$$

$$[\mathrm{O_{2,ads}}] = K_{\mathrm{O_2}}[\mathrm{site_{O_2}}]C_{\mathrm{O_2}} \tag{9}$$

where $[j_{\mathrm{ads}}]$ represents the concentration of the species j (j = 4-CP, 4-CC, HQ, and O_2) adsorbed on the catalyst surface, K_j is the equilibrium adsorption constant, $[\mathrm{site}_j]$ represents the superficial concentration of vacant adsorption sites, and C_j is the concentration of j in the suspension bulk.

By making a balance of sites and employing the above equations, it is possible to relate the concentration of vacant sites to the total concentration of sites, $[\mathrm{site}_{j,\mathrm{T}}]$:

$$[\mathrm{site_{4\text{-}CP}}] = \frac{[\mathrm{site_{4\text{-}CP,T}}]}{1 + K_{\text{4-CP}}C_{\text{4-CP}} + K_{\text{4-CC}}C_{\text{4-CC}} + K_{\mathrm{HQ}}C_{\mathrm{HQ}}} \tag{10}$$

$$[\mathrm{site_{O_2}}] = \frac{[\mathrm{site_{O_2,T}}]}{1 + K_{\mathrm{O_2}}C_{\mathrm{O_2}}} \tag{11}$$

Considering that the hydroxyl radical attack is the main route for the degradation of 4-CP and the organic intermediates [10,12], the superficial degradation rate of i (i = 4-CP, 4-CC, and HQ) can be represented by the following expression:

$$r_i = k_i[^{\bullet}\mathrm{OH}][i_{\mathrm{ads}}] \tag{12}$$

where k_i is the kinetic constant of the reaction between the organic compound and hydroxyl radicals, $[^{\bullet}\mathrm{OH}]$ is the concentration of hydroxyl radicals on the surface of the TiO_2 particles, and $[i_{\mathrm{ads}}]$ represents the superficial concentration of i.

By applying the kinetic micro-steady state approximation for the concentration of electrons, holes and hydroxyl radicals [2], we obtain the following expressions:

$$r_{\mathrm{e^-}} = r_{\mathrm{gs}} - k_2[\mathrm{e^-}][\mathrm{h^+}] - k_3[\mathrm{e^-}][\mathrm{O_{2,ads}}] \approx 0 \tag{13}$$

$$r_{\mathrm{h^+}} = r_{\mathrm{gs}} - k_2[\mathrm{e^-}][\mathrm{h^+}] - k_4[\mathrm{h^+}][\mathrm{H_2O_{ads}}] \approx 0 \tag{14}$$

$$r_{^{\bullet}\mathrm{OH}} = k_4[\mathrm{h^+}][\mathrm{H_2O_{ads}}] - \sum_i k_i[^{\bullet}\mathrm{OH}][i_{\mathrm{ads}}] - \sum_l k''_l[^{\bullet}\mathrm{OH}][\mathrm{Y}_{l,\mathrm{ads}}] \approx 0 \tag{15}$$

where $r_{\mathrm{e^-}}$, $r_{\mathrm{h^+}}$, and $r_{^{\bullet}\mathrm{OH}}$ correspond to the reaction rate of electrons, holes and hydroxyl radicals, respectively. The superficial rate of electron–hole generation, r_{gs}, is given by [31]

$$r_{\mathrm{gs}}(\mathbf{x}) = \frac{\bar{\phi}}{a_{\mathrm{v}}}\int_{\lambda} e^{\mathrm{a}}_{\lambda}(\mathbf{x})\,\mathrm{d}\lambda \tag{16}$$

where e^{a}_{λ} represents the local volumetric rate of photon absorption (LVRPA) and $\bar{\phi}$ is the primary quantum yield averaged over the wavelength range.

Additional assumptions have been made to simplify the model [2,27,31]: (i) there are no mass transport limitations, (ii) oxygen concentration is constant and in excess with respect to the stoichiometric demand, and (iii) the concentration of water molecules and hydroxyl ions on the catalytic surface remains constant.

On the basis of these considerations, and by employing Eqs. (6)–(16), we derived the following expressions:

$$r_{\text{4-CP,1}}(\mathbf{x},t) = \frac{\alpha_{2,1}C_{\text{4-CP}}(t)}{1 + \alpha_3 C_{\text{4-CP}}(t) + \alpha'_1 C_{\text{4-CC}}(t) + \alpha'_2 C_{\mathrm{HQ}}(t)} \times \left(-1 + \sqrt{1 + \frac{\alpha_1}{a_{\mathrm{v}}}e^{\mathrm{a}}(\mathbf{x})}\right) \tag{17}$$

$$r_{\text{4-CP,2}}(\mathbf{x},t) = \frac{\alpha_{2,2}C_{\text{4-CP}}(t)}{1 + \alpha_3 C_{\text{4-CP}}(t) + \alpha'_1 C_{\text{4-CC}}(t) + \alpha'_2 C_{\mathrm{HQ}}(t)} \times \left(-1 + \sqrt{1 + \frac{\alpha_1}{a_{\mathrm{v}}}e^{\mathrm{a}}(\mathbf{x})}\right) \tag{18}$$

$$r_{\text{4-CC}}(\mathbf{x},t) = \frac{\alpha_4 C_{\text{4-CC}}(t)}{1 + \alpha_3 C_{\text{4-CP}}(t) + \alpha'_1 C_{\text{4-CC}}(t) + \alpha'_2 C_{\mathrm{HQ}}(t)} \times \left(-1 + \sqrt{1 + \frac{\alpha_1}{a_{\mathrm{v}}}e^{\mathrm{a}}(\mathbf{x})}\right) \tag{19}$$

$$r_{\mathrm{HQ}}(\mathbf{x},t) = \frac{\alpha_5 C_{\mathrm{HQ}}(t)}{1 + \alpha_3 C_{\text{4-CP}}(t) + \alpha'_1 C_{\text{4-CC}}(t) + \alpha'_2 C_{\mathrm{HQ}}(t)} \times \left(-1 + \sqrt{1 + \frac{\alpha_1}{a_{\mathrm{v}}}e^{\mathrm{a}}(\mathbf{x})}\right) \tag{20}$$

where α_1, $\alpha_{2,1}$, $\alpha_{2,2}$, α_3, α_4, α_5, α'_1, and α'_2 represent intrinsic kinetic parameters. A detailed derivation of the above equations can be found in Appendix A.

3.3. Radiation model

The first step in the photocatalytic degradation of 4-CP is the activation of TiO_2 by photon absorption in the UV range.

Therefore, the knowledge of the radiation field inside the reactor is essential to model the kinetics of the photocatalytic system. A rigorous approach to obtain the spatial and directional distributions of radiation intensities results from the application of the RTE to the heterogeneous system under study.

The main changes in the spatial distribution of radiation inside the employed reactor occur along the x coordinate axis (Fig. 2a), due to the extinction produced by the catalyst particles. This effect allows us to model the radiation propagation with only one spatial variable (x). Also, the arrangement of the lamps and the ground glass plates ensure the arrival of diffuse radiation with azimuthal symmetry at the reactor windows. Therefore, radiation can be modeled with one angular variable (θ) [32]. The one-dimensional, one-directional radiation transport model, applied to solve the RTE in the photocatalytic reactor, yields [33]

$$\mu \frac{\partial I_\lambda(x,\mu)}{\partial x} + \beta_\lambda I_\lambda(x,\mu) = \frac{\sigma_\lambda}{2} \int_{\mu'=-1}^{1} I_\lambda(x,\mu')\, p(\mu,\mu')\, \mathrm{d}\mu' \tag{21}$$

where I_λ is the spectral radiation intensity; λ represents the radiation wavelength; x, is the axial coordinate; σ_λ, the volumetric scattering coefficient; μ, the direction cosine of the ray for which the RTE is written ($\mu = \cos\theta$); μ', the cosine of an arbitrary ray before scattering; and p represents the phase function for scattering. The Henyey and Greenstein phase function ($P_{\mathrm{HG},\lambda}$) was adopted to model the radiation scattering over TiO_2 particles [34]:

$$p_{\mathrm{HG},\lambda}(\mu_0) = \frac{1 - g_\lambda^2}{(1 + g_\lambda^2 - 2g_\lambda\mu_0)^{3/2}} \tag{22}$$

where g_λ is a free parameter called the asymmetry factor, and μ_0 represents the cosine of the angle between the direction of the incident and the scattered rays.

The effects of reflection, refraction and absorption of radiation at the reactor windows were taken into account to obtain the boundary conditions for Eq. (21). At $x = 0$ and $x = L_R$ (Fig. 2a), radiation intensities are the result of two contributions: (i) the transmitted portion of the radiation coming from the lamps ($I_{0,\lambda}$ at $x = 0$ and $I_{L_R,\lambda}$ at $x = L_R$), and (ii) the reflected portion of the radiation coming from the suspension ($\Gamma_{W,\lambda} I_\lambda$, where $\Gamma_{W,\lambda}$ is the global reflection coefficient of the reactor windows). As a consequence of refraction, the angular directions of the specific intensities that enter the reactor are limited by the critical angle of total reflection, θ_c. Then, the boundary conditions of the RTE result

$$I_\lambda(0,\mu) = \Gamma_{W,\lambda}(-\mu) I_\lambda(0,-\mu) \quad 0 \le \mu < \mu_c \tag{23}$$

$$I_\lambda(0,\mu) = I_{0,\lambda} + \Gamma_{W,\lambda}(-\mu) I_\lambda(0,-\mu) \quad \mu_c \le \mu \le 1 \tag{24}$$

$$I_\lambda(L_R,-\mu) = \Gamma_{W,\lambda}(\mu) I_\lambda(L_R,\mu) \quad 0 \le \mu < \mu_c \tag{25}$$

$$I_\lambda(L_R,-\mu) = I_{L_R,\lambda} + \Gamma_{W,\lambda}(\mu) I_\lambda(L_R,\mu) \quad \mu_c \le \mu \le 1 \tag{26}$$

where $\mu_c = \cos\theta_c$. More details concerning the radiation model can be found elsewhere [24].

The values of g_λ and the specific coefficients (per catalyst mass concentration C_m) β^*_λ and σ^*_λ were calculated employing the method described in a previous work [35]. The discrete ordinate method [36] was applied to solve the radiation model. This method involves the spatial and directional discretization

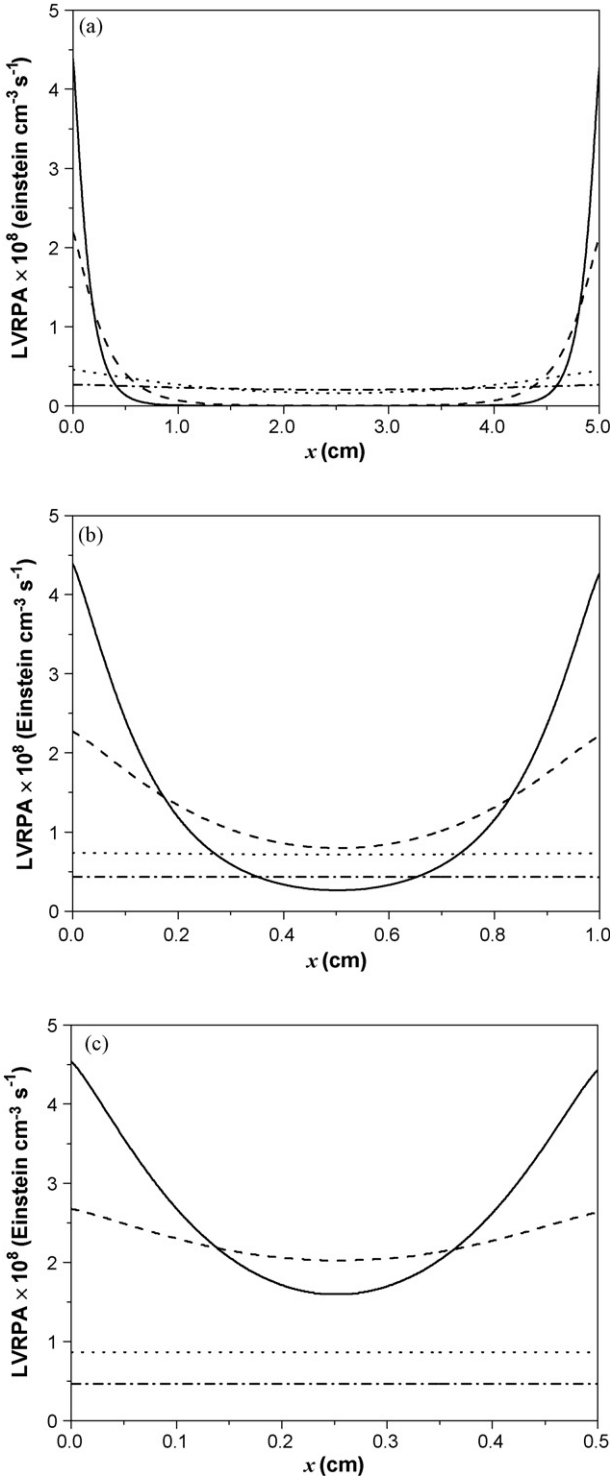

Fig. 6. LVRPA profiles for different catalyst concentrations and different reactor lengths. (—): $C_m = 1.0 \times 10^{-3}$ g cm^{-3}; (- - -): $C_m = 0.5 \times 10^{-3}$ g cm^{-3}; (· · ·): $C_m = 0.1 \times 10^{-3}$ g cm^{-3}; (- · -): $C_m = 0.05 \times 10^{-3}$ g cm^{-3}. (a) $L_R = 5.0$ cm, (b) $L_R = 1.0$ cm, (c) $L_R = 0.5$ cm.

of the RTE, transforming Eq. (21) into a set of algebraic equations that can be solved numerically. The solution of the RTE provides the spectral radiation intensity at each point and each direction inside the reactor.

Once the spectral intensities were obtained, the LVRPA, involved in the reaction rate expressions, was computed as

$$e^{a}(x) = 2\pi \int_{\lambda} \kappa_{\lambda} \int_{\mu=-1}^{1} I_{\lambda}(x,\mu)\, d\mu\, d\lambda \qquad (27)$$

where κ_λ is the volumetric absorption coefficient.

The LVRPA profiles for different TiO_2 concentrations, and for the three values of L_R employed in the experiments, are shown in Fig. 6. The strongest variations of photon absorption inside the reactor are observed with the highest catalyst concentrations ($C_m \geq 0.5 \times 10^{-3}$ g cm^{-3}) and for $L_R = 5.0$ cm (Fig. 6a). As long as the TiO_2 concentration decreases and the reactor becomes thinner, more uniform profiles are obtained.

4. Results and discussion

4.1. Typical experimental results

Fig. 7 illustrates the changes in the UV absorption spectra of the reacting solution at different irradiation times. The spectra correspond to the degradation of 4-CP performed with $C_m = 1.0 \times 10^{-3}$ g cm^{-3}, $Q_L = 100\%$ and $L_R = 5.0$ cm. At $t = 0$, the spectrum is coincident with that of pure 4-CP. As long as the reaction progresses, the characteristic peaks of 4-CP at $\lambda = 280$ nm and $\lambda = 225$ nm decrease significantly. A parallel increment of the absorbance near 250 nm can be attributed to the formation of intermediates.

Fig. 8 depicts the evolution of the experimental concentrations of 4-CP and the intermediate products for the same run. As can be observed in the figure, 4-CP gradually decreases throughout the experiment, and it is almost completely degraded at the end of the run. 4-CC and HQ initially increase their concentration, reach a maximum value and then decay slowly until they nearly disappear after 8 h of irradiation. The concentration level of BQ remains very low and never reaches significant values.

The changes in TOC, chloride ions concentration and pH, corresponding to the above-cited run, are reported in Fig. 9. TOC concentration has been expressed as molar concentration of organic carbon divided by 6 (TOC/6), considering that the substrate and the main intermediates contain six carbon atoms. The TOC/6 concentration decreases slowly and an important amount remains in the samples even after all aromatic intermediates have been degraded. This may be attributed to the presence of aliphatic compounds that are not detected by HPLC analysis, such as aldehydes and carboxylic acids [12]. Also, a gradual release of chloride ions into the reacting suspension is detected during the photodegradation of 4-CP. After 10 h of irradiation, the concentration of Cl^- practically reaches the concentration of chlorine atoms initially present in the molecules of 4-CP (not shown in the figure). This indicates that no chlorinated compounds remain in solution after the photocatalytic experiment. The pH of the mixture does not vary substantially during the reaction time. This is a significant aspect, since important changes in the pH affects the reaction rate and the optical properties of TiO_2 [24].

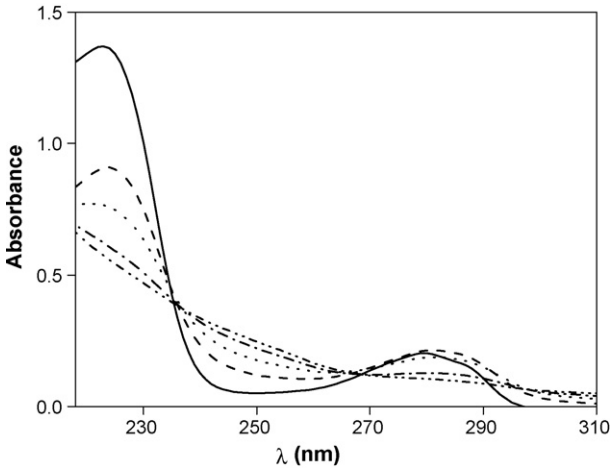

Fig. 7. UV spectra of the reacting mixture during a typical photocatalytic experiment. (—): $t = 0$; (- - -): $t = 1$ h; (· · ·): $t = 2$ h; (- · -): $t = 4$ h; (- · · -): $t = 6$ h.

4.2. Kinetic parameters estimation

A Levenberg–Marquardt optimization algorithm was applied to estimate the kinetic parameters involved in Eqs. (17)–(20). The experimental concentrations of 4-CP, 4-CC and HQ, obtained from samples at different reaction times, were compared with simulation results. The optimization procedure renders the values of the parameters that minimize the differences between predicted concentrations and experimental data. From the results of the optimization algorithm it was found that, under the operating conditions of the experiments, the terms $\alpha_3 C_{4\text{-CP}}(t)$, $\alpha'_1 C_{4\text{-CC}}(t)$, and $\alpha'_2 C_{HQ}(t)$, in the denominator of the kinetic equations, were two orders of magnitude lower than 1, and thus could be neglected.

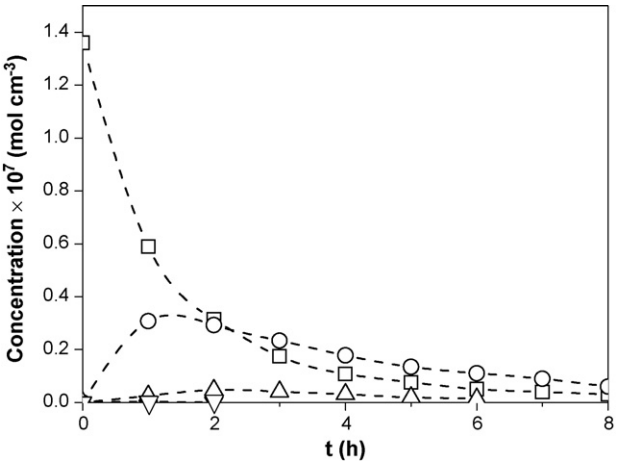

Fig. 8. Evolution of the concentration of 4-CP and of the main intermediate products during a typical photocatalytic experiment. (□) 4-CP; (○) 4-CC; (△) HQ; (▽) BQ.

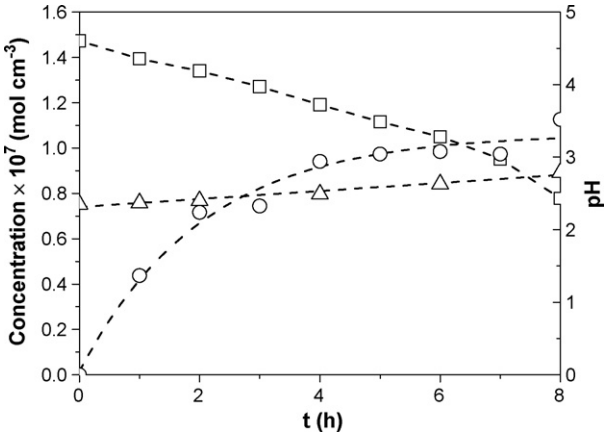

Fig. 9. Evolution of TOC, chloride concentration and pH during a typical photocatalytic experiment. (□) TOC/6; (○) chloride ion; (△) pH.

Consequently, the degradation rates follow a first order kinetics with respect to the substrate concentration. The final expressions employed for the parameters estimation were the following:

$$r_{4\text{-CP},1}(x,t) = \alpha_{2,1} C_{4\text{-CP}}(t)\left(-1+\sqrt{1+\frac{\alpha_1}{a_v}e^a(x)}\right) \quad (28)$$

$$r_{4\text{-CP},2}(x,t) = \alpha_{2,2} C_{4\text{-CP}}(t)\left(-1+\sqrt{1+\frac{\alpha_1}{a_v}e^a(x)}\right) \quad (29)$$

$$r_{4\text{-CC}}(x,t) = \alpha_4 C_{4\text{-CC}}(t)\left(-1+\sqrt{1+\frac{\alpha_1}{a_v}e^a(x)}\right) \quad (30)$$

$$r_{HQ}(x,t) = \alpha_5 C_{HQ}(t)\left(-1+\sqrt{1+\frac{\alpha_1}{a_v}e^a(x)}\right) \quad (31)$$

The values of the five kinetic parameters, with the corresponding 95% confidence interval, are reported in Table 4. The value of $\alpha_{2,1}$ is almost 5 times greater than that of $\alpha_{2,2}$. This result, in agreement with the experiments, points out that the degradation of 4-CP via 4-CC is favored, being 4-CC the most abundant primary intermediate. On the other hand, the kinetic parameters α_4 and α_5 are very similar. As a consequence, for a given concentration of the intermediate species, the photocatalytic degradation rates of 4-CC and HQ are comparable.

Figs. 10 and 11 depict the experimental and predicted concentrations of 4-CP, 4-CC, and HQ under different operating conditions. Symbols correspond to experimental data. Model predictions, represented by solid lines, where calculated employing Eqs. (3)–(5) and Eqs. (28)–(31), with the corresponding kinetic parameters presented in Table 4. Fig. 10 shows results for $L_R = 1.0$ cm, $Q_L = 100\%$, and three TiO_2 concentrations. As can be observed in the figure, the degradation rate of 4-CP increases with the catalyst loading. For $C_m = 0.05 \times 10^{-3}$ g cm^{-3} (Fig. 10c), the conversion of 4-CP after 8 h of irradiation reaches 60%. For $C_m = 0.1 \times 10^{-3}$ g cm^{-3} (Fig. 10b), the conversion increases up to 80%, whereas at the highest catalyst concentration, $C_m = 1.0 \times 10^{-3}$ g cm^{-3} (Fig. 10a), the degradation is complete at the end of the run. The intermediate products reaction rates follow a similar behavior. For the lowest catalyst loading, 4-CC and HQ gradually increase their concentration throughout the run. For $C_m = 0.1 \times 10^{-3}$ g cm^{-3}, the intermediates reach a maximum value after 5–6 h and then start to decline slowly. For $C_m = 1.0 \times 10^{-3}$ g cm^{-3}, the concentrations of 4-CC and HQ initially rise, reach a maximum around the first hour, and then decrease until they almost disappear at the end of the run.

Fig. 11 reports results for $C_m = 0.5 \times 10^{-3}$ g cm^{-3}, $Q_L = 100\%$, and different values of L_R. The model could accurately predict the evolution of 4-CP, 4-CC and HQ under very different conditions of optical thickness, with important dark regions in the reactor with $L_R = 5.0$ cm (Fig. 11a) and almost uniform irradiation with $L_R = 0.5$ cm (Fig. 11c).

Considering all the runs, good agreement was obtained between model predictions and experimental data. The root mean square error (RMSE) of the estimations was computed as

$$\text{RMSE} = \sqrt{\frac{1}{N}\sum_{i=1}^{N}\left(\frac{C_{i,\text{exp}} - C_i}{C_{i,\text{exp}}}\right)^2} \times 100 \quad (32)$$

where $C_{i,\text{exp}}$ and C_i are the experimental and model concentrations of the organic compounds, respectively, and N is the total number of samples for the complete set of experimental runs. The values of concentration lower than 2.0×10^{-8} mol cm^{-3} were excluded from calculations because they were comprised in the range of instrumental error. The RMSE was 14.4%.

It is worth noting that the dependence of reaction kinetics on the photon absorption rate, given by the term $\psi = (-1 + \sqrt{1 + (\alpha_1/a_v)e^a(x)})$ in Eqs. (28)–(31), can take two limiting values. For high radiation levels, and sufficiently high values of e^a, it holds $(\alpha_1/a_v)e^a(x) \gg 1$ and $\sqrt{1 + (\alpha_1/a_v)e^a(x)} \approx \sqrt{(\alpha_1/a_v)e^a(x)}$. In addition, if $\sqrt{(\alpha_1/a_v)e^a(x)} \gg 1$, then $\psi \approx \sqrt{(\alpha_1/a_v)e^a(x)}$. Therefore, the reaction rate is proportional to the square root of the photon absorption rate under high radiation conditions. On the contrary, when radiation levels are low and $(\alpha_1/a_v)e^a(x) \ll 1$, it can be proved, using a Taylor series expansion [31], that

Table 4
Estimated kinetic parameters

Parameter	α_1	$\alpha_{2,1}$	$\alpha_{2,2}$	α_4	α_5
Value	1.09×10^{11}	9.43×10^{-6}	2.18×10^{-6}	1.29×10^{-5}	9.21×10^{-6}
Confidence interval (95%)	$\pm 0.07 \times 10^{11}$	$\pm 0.26 \times 10^{-6}$	$\pm 0.46 \times 10^{-6}$	$\pm 0.08 \times 10^{-5}$	$\pm 0.96 \times 10^{-6}$
Units	s cm^2 Einstein^{-1}	cm s^{-1}	cm s^{-1}	cm s^{-1}	cm s^{-1}

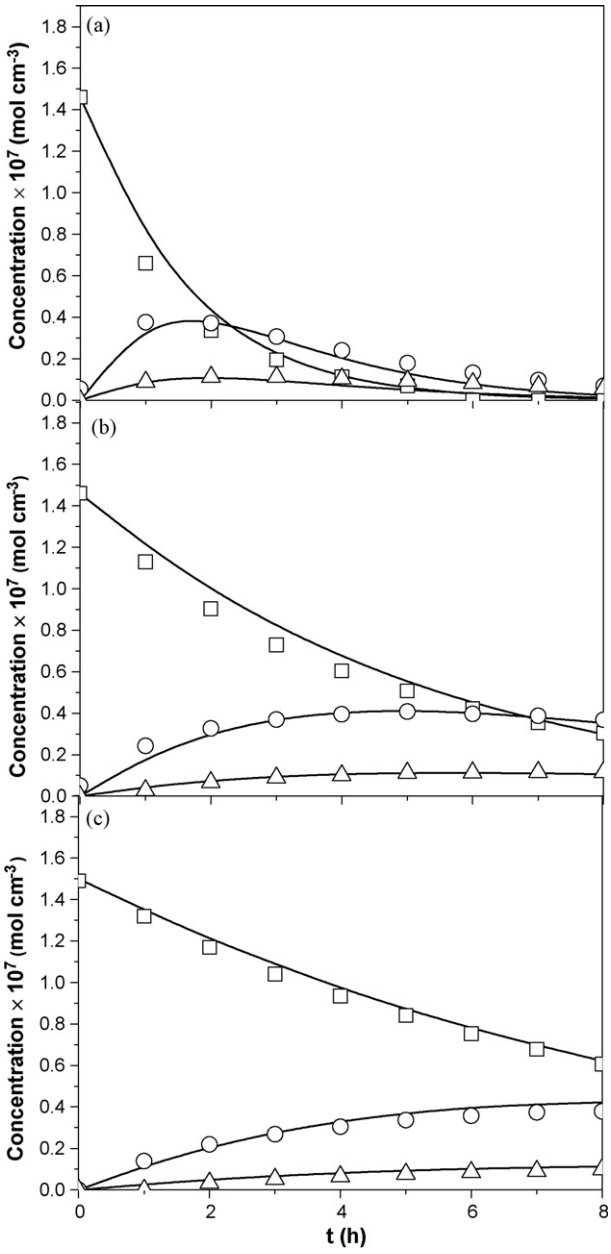

Fig. 10. Experimental and predicted concentrations of 4-CP, 4-CC, and HQ vs. time for L_R = 1.0 cm, Q_L = 100% and different C_m. Experimental data: (□) 4-CP; (○) 4-CC; (△) HQ. Model results: solid lines. (a) $C_m = 1.0 \times 10^{-3}$ g cm^{-3}; (b) $C_m = 0.1 \times 10^{-3}$ g cm^{-3}; (c) $C_m = 0.05 \times 10^{-3}$ g cm^{-3}.

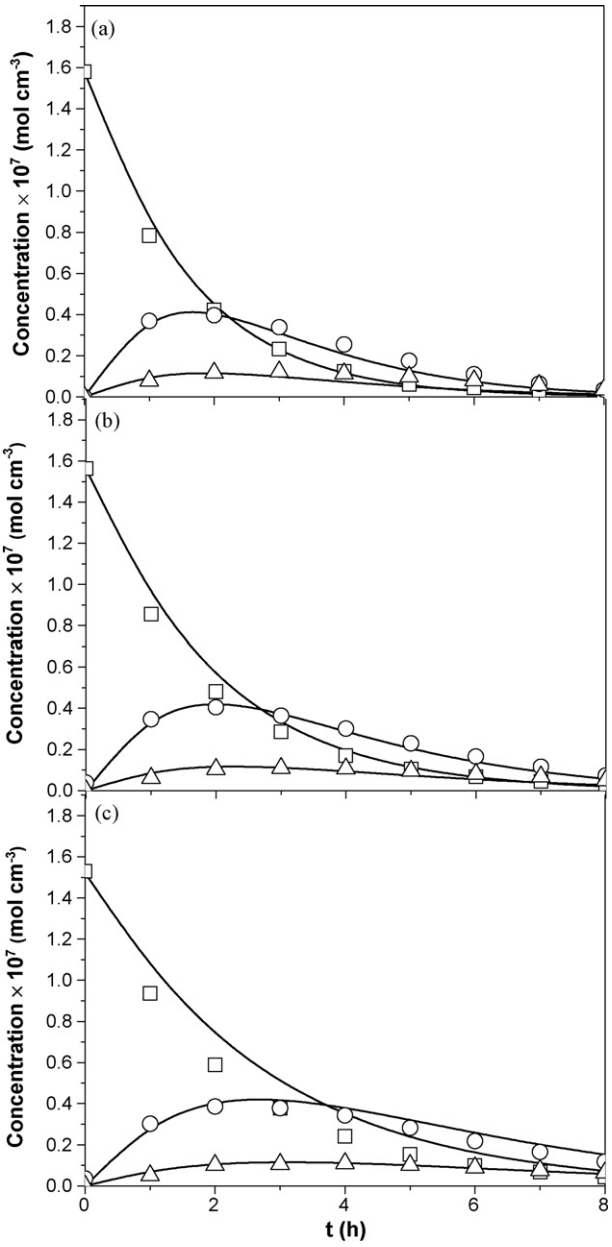

Fig. 11. Experimental and predicted concentrations of 4-CP, 4-CC, and HQ vs. time for $C_m = 0.5 \times 10^{-3}$ g cm^{-3}, Q_L = 100% and different L_R. Experimental data: (□) 4-CP; (○) 4-CC; (△) HQ. Model results: solid lines. (a) L_R = 5.0 cm; (b) L_R = 1.0 cm; (c) L_R = 0.5 cm.

$\sqrt{1+(\alpha_1/a_v)e^a(x)} \approx 1 + 1/2(\alpha_1/a_v)e^a(x)$. Hence, $\psi \approx 1/2(\alpha_1/a_v)e^a(x)$ and it is demonstrated that the dependence of the reaction rate on the photon absorption rate results linear for low radiation conditions.

Both limiting cases can be clearly found in the photocatalytic reactor employed in this work. Numerical information for two experimental conditions is given in Table 5. For a reactor length of L_R = 5.0 cm and $C_m = 1.0 \times 10^{-3}$ g cm^{-3}, the reactor is highly irradiated at $x = 0$ (see Fig. 6a). In this case, as shown in the first row of Table 5, the term $(\alpha_1/a_v)e^a(x) \gg 1$ and $\sqrt{(\alpha_1/a_v)e^a(x)} > 1$. As a result, the dependence of the reaction rate is nearly proportional to the square root of e^a. For the same experimental conditions but in the center of the reactor ($x = L_R/2$), as shown in the second row of the table, the level of irradiation is extremely low and the term $(\alpha_1/a_v)e^a(x) \ll 1$. Therefore, the dependence of the reaction kinetics with the photon absorption rate is linear. For a reactor length of L_R = 0.5 cm and $C_m = 0.05 \times 10^{-3}$ g cm^{-3}, the reactor is uniformly illuminated (see Fig. 6c), with $(\alpha_1/a_v)e^a(x) \gg 1$. Consequently, the reaction rate can be considered proportional to the square root of the photon absorption rate throughout the reaction space. These results show that in the same photocatalytic slurry reactor, high, intermediate, and low absorption levels can coexist. For that

Table 5
Dependence of the reaction rate on the photon absorption rate

L_R (cm)	C_m ($\times 10^3$ g cm^{-3})	x	$\frac{\alpha_1}{a_v} e^a(x)$	$\sqrt{\frac{\alpha_1}{a_v} e^a(x)}$
5	1.0	0	49.7	7.05
5	1.0	$L_R/2$	1.15×10^{-4}	1.07×10^{-2}
0.5	0.05	0	105.6	10.3
0.5	0.05	$L_R/2$	105.6	10.3

reason, the complete expression of ψ in the reaction rate equations must be used.

5. Conclusions

A kinetic model to represent the photocatalytic degradation of 4-CP in a slurry reactor has been developed. It is based on a reaction scheme that postulates the $^{\bullet}$OH as the main oxidant in the pollutant degradation. A precise evaluation of the radiation field inside the reactor, required to model the effect of the radiation absorption on the reaction rate, was obtained by applying the radiative transfer equation to the system.

The kinetic model predicts the time evolution of 4-CP and the two main reaction intermediates, 4-CC and HQ, under different operating conditions that include the variation of the irradiation level, the reactor length, and the catalyst concentration. The five intrinsic kinetic parameters of the model were estimated by means of a Levenberg–Marquardt optimization algorithm. Good agreement was obtained between model predictions and experimental data, with a root mean square error of 14.4%.

Acknowledgments

The authors are grateful to Universidad Nacional del Litoral (UNL), Consejo Nacional de Investigaciones Científicas y Técnicas (CONICET) and Agencia Nacional de Promoción Científica y Tecnológica (ANPCyT) for the financial support.

They also thank Antonio C. Negro for his valuable help during the experimental work.

Appendix A

The degradation rate of 4-CP, as postulated in Section 3.2, is the result of the reaction between hydroxyl radicals and adsorbed molecules of 4-CP. Following Eq. (12), and considering the parallel degradation path to give 4-CC and HQ, the degradation rate of 4-CP can be represented as

$$r_{4\text{-CP}} = k_5[^{\bullet}\text{OH}][\text{4-CP}_{ads}] + k_6[^{\bullet}\text{OH}][\text{4-CP}_{ads}] \quad \text{(I.1)}$$

$$r_{4\text{-CP}} = (k_5 + k_6)[^{\bullet}\text{OH}][\text{4-CP}_{ads}] \quad \text{(I.2)}$$

From Eqs. (13) to (15), the following expressions for the concentration of electrons, holes and hydroxyl radicals can be obtained:

$$[e^-] = \frac{r_{gs}}{k_2[h^+] + k_3[O_{2,ads}]} \quad \text{(I.3)}$$

$$[h^+] = \frac{r_{gs}}{k_2[e^-] + k_4[H_2O_{ads}]} \quad \text{(I.4)}$$

$$[^{\bullet}\text{OH}] = \frac{k_4[h^+][H_2O_{ads}]}{(k_5 + k_6)[\text{4-CP}_{ads}] + k_7[\text{4-CC}_{ads}] + k_8[\text{HQ}_{ads}] + \sum_l k_l''[Y_{l,ads}]} \quad \text{(I.5)}$$

Introducing Eq. (I.3) into Eq. (I.4), results the following quadratic expression:

$$[h^+]^2 + \frac{k_3[O_{2,ads}]}{k_2}[h^+] - \frac{r_{gs}k_3[O_{2,ads}]}{k_4[H_2O_{ads}]k_2} = 0 \quad \text{(I.6)}$$

From the solution of Eq. (I.6), the expression for the hole concentration is obtained (the positive root is the only one that has physical meaning):

$$[h^+] = \left\{ -1 + \sqrt{1 + \frac{4r_{gs}k_2}{k_4k_3[H_2O_{ads}][O_{2,ads}]}} \right\} \frac{k_3[O_{2,ads}]}{2k_2} \quad \text{(I.7)}$$

Introducing Eq. (I.7) into Eq. (I.5), results

$$[^{\bullet}\text{OH}] = \frac{k_4k_3[H_2O_{ads}][O_{2,ads}]\{-1 + \sqrt{1 + (4r_{gs}k_2/k_4k_3[H_2O_{ads}][O_{2,ads}])}\}}{2k_2\{(k_5 + k_6)[\text{4-CP}_{ads}] + k_7[\text{4-CC}_{ads}] + k_8[\text{HQ}_{ads}] + \sum_l k_l''[Y_{l,ads}]\}} \quad \text{(I.8)}$$

Then, introducing the above expression of [$^{\bullet}$OH] into Eq. (I.2), we arrive to the following equation:

$$r_{4\text{-CP}} = \frac{(k_5 + k_6)k_4k_3[H_2O_{ads}][O_{2,ads}][\text{4-CP}_{ads}]\left\{ -1 + \sqrt{1 + (4r_{gs}k_2/k_4k_3[H_2O_{ads}][O_{2,ads}])} \right\}}{2k_2\left\{ (k_5 + k_6)[\text{4-CP}_{ads}] + k_7[\text{4-CC}_{ads}] + k_8[\text{HQ}_{ads}] + \sum_l k_l''[Y_{l,ads}] \right\}} \quad \text{(I.9)}$$

Assuming that the concentration of oxygen and water on the catalytic surface remain constant, and that the consumption of

hydroxyl radicals by inorganic species Y_l is also constant [27], Eq. (I.9) can be rewritten as

$$r_{4\text{-CP}} = \frac{(\delta_{2,1} + \delta_{2,2})[4\text{-CP}_{ads}]\{-1 + \sqrt{1 + \delta_1 r_{gs}}\}}{\delta_3\{(k_5 + k_6)[4\text{-CP}_{ads}] + k_7[4\text{-CC}_{ads}] + k_8[HQ_{ads}]\} + 1} \quad (I.10)$$

where

$$\delta_1 = \frac{4k_2}{k_4 k_3 [H_2O_{ads}][O_{2,ads}]} \quad (I.11)$$

$$\delta_{2,1} = \frac{k_5 k_4 k_3 [H_2O_{ads}][O_{2,ads}]}{2k_2\left(\sum_l k_l'' [Y_{l,ads}]\right)} \quad (I.12)$$

$$\delta_{2,2} = \frac{k_6 k_4 k_3 [H_2O_{ads}][O_{2,ads}]}{2k_2\left(\sum_l k_l'' [Y_{l,ads}]\right)} \quad (I.13)$$

$$\delta_3 = \frac{1}{\sum_l k_l'' [Y_{l,ads}]} \quad (I.14)$$

Substituting $[4\text{-CP}_{ads}]$, $[4\text{-CC}_{ads}]$, and $[HQ_{ads}]$ in Eq. (I.10) by the corresponding equilibrium expressions (Eqs. (6)–(8)), and rearranging, we obtain

$$r_{4\text{-CP}} = \frac{(\delta_{2,1} + \delta_{2,2})K_{4\text{-CP}}C_{4\text{-CP}}\{-1 + \sqrt{1 + \delta_1 r_{gs}}\}}{\delta_3\{(k_5 + k_6)K_{4\text{-CP}}C_{4\text{-CP}} + k_7 K_{4\text{-CC}}C_{4\text{-CC}} + k_8 K_{HQ}C_{HQ}\} + 1/[site_{4\text{-CP}}]} \quad (I.15)$$

Introducing Eq. (10), that represents the concentration of vacant sites for 4-CP, into (I.15), and rearranging, results

$$r_{4\text{-CP}} = \frac{(\delta_{2,1} + \delta_{2,2})[site_{4\text{-CP,T}}]K_{4\text{-CP}}C_{4\text{-CP}}(-1 + \sqrt{1 + \delta_1 r_{gs}})}{1 + \{[site_{4\text{-CP,T}}]\delta_3(k_5 + k_6)K_{4\text{-CP}} + K_{4\text{-CP}}\}C_{4\text{-CP}} + \{[site_{4\text{-CP,T}}]\delta_3 k_7 K_{4\text{-CC}} + K_{4\text{-CC}}\}C_{4\text{-CC}} + \{[site_{4\text{-CP,T}}]\delta_3 k_8 K_{HQ} + K_{HQ}\}C_{HQ}} \quad (I.16)$$

The superficial concentration of sites $[site_{4\text{-CP,T}}]$, per unit area of catalyst, can be considered constant. Also, introducing Eq. (16) into Eq. (I.16), and defining $e^a = \int_\lambda e^a_\lambda \, d\lambda$, we obtain

$$r_{4\text{-CP}} = \frac{(\alpha_{2,1} + \alpha_{2,2})C_{4\text{-CP}}}{1 + \alpha_3 C_{4\text{-CP}} + \alpha_1' C_{4\text{-CC}} + \alpha_2' C_{HQ}} \times \left(-1 + \sqrt{1 + \frac{\alpha_1}{a_v} e^a}\right) \quad (I.17)$$

where

$$\alpha_1 = \delta_1 \bar{\phi} \quad (I.18)$$

$$\alpha_{2,1} = \delta_{2,1}[site_{4\text{-CP,T}}]K_{4\text{-CP}} \quad (I.19)$$

$$\alpha_{2,2} = \delta_{2,2}[site_{4\text{-CP,T}}]K_{4\text{-CP}} \quad (I.20)$$

$$\alpha_3 = \delta_3[site_{4\text{-CP,T}}](k_5 + k_6)K_{4\text{-CP}} + K_{4\text{-CP}} \quad (I.21)$$

$$\alpha_1' = \delta_3[site_{4\text{-CP,T}}]k_7 K_{4\text{-CC}} + K_{4\text{-CC}} \quad (I.22)$$

$$\alpha_2' = \delta_3[site_{4\text{-CP,T}}]k_8 K_{HQ} + K_{HQ} \quad (I.23)$$

Then, the degradation rate of 4-CP can be divided into the next equations:

$$r_{4\text{-CP},1} = \frac{\alpha_{2,1}C_{4\text{-CP}}}{1 + \alpha_3 C_{4\text{-CP}} + \alpha_1' C_{4\text{-CC}} + \alpha_2' C_{HQ}} \times \left(-1 + \sqrt{1 + \frac{\alpha_1}{a_v} e^a}\right) \quad (I.24)$$

$$r_{4\text{-CP},2} = \frac{\alpha_{2,2}C_{4\text{-CP}}}{1 + \alpha_3 C_{4\text{-CP}} + \alpha_1' C_{4\text{-CC}} + \alpha_2' C_{HQ}} \times \left(-1 + \sqrt{1 + \frac{\alpha_1}{a_v} e^a}\right) \quad (I.25)$$

By following a similar analysis, the degradation rates for 4-CC and HQ can be obtained:

$$r_{4\text{-CC}} = \frac{\alpha_4 C_{4\text{-CC}}}{1 + \alpha_3 C_{4\text{-CP}} + \alpha_1' C_{4\text{-CC}} + \alpha_2' C_{HQ}} \times \left(-1 + \sqrt{1 + \frac{\alpha_1}{a_v} e^a}\right) \quad (I.26)$$

$$r_{HQ} = \frac{\alpha_5 C_{HQ}}{1 + \alpha_3 C_{4\text{-CP}} + \alpha_1' C_{4\text{-CC}} + \alpha_2' C_{HQ}} \times \left(-1 + \sqrt{1 + \frac{\alpha_1}{a_v} e^a}\right) \quad (I.27)$$

where

$$\alpha_4 = \frac{k_7 k_4 k_3 [H_2O_{ads}][O_{2,ads}][site_{4\text{-CP,T}}]K_{4\text{-CC}}}{2k_2\left(\sum_l k_l'' [Y_{l,ads}]\right)} \quad (I.28)$$

$$\alpha_5 = \frac{k_8 k_4 k_3 [H_2O_{ads}][O_{2,ads}][site_{4\text{-CP,T}}]K_{HQ}}{2k_2\left(\sum_l k_l'' [Y_{l,ads}]\right)} \quad (I.29)$$

References

[1] R.W. Matthews, J. Catal. 111 (1988) 264.
[2] C.S. Turchi, D.F. Ollis, J. Catal. 122 (1990) 178.
[3] D.W. Bahnemann, J. Cunningham, M.A. Fox, E. Pelizzetti, P. Pichat, N. Serpone, in: G.R. Helz, R.G. Zepp, D.G. Crosby (Eds.), Aquatic and Surface Photochemistry, F.L. Lewis Publishers, Boca Raton, 1994 , p. 261.
[4] M.R. Hoffmann, S.T. Martin, W. Choi, D.W. Bahnemann, Chem. Rev. 95 (1995) 69.
[5] J.M. Herrmann, Catal. Today 53 (1999) 115.
[6] M. Pera-Titus, V. García Molina, M.A. Baños, J. Giménez, S. Esplugas, Appl. Catal. B 47 (2004) 219.
[7] H. Al-Ekabi, N. Serpone, E. Pelizzetti, C. Minero, M.A. Fox, R.B. Draper, Langmuir 5 (1989) 250.
[8] R.W. Matthews, Water Res. 24 (1990) 653.

[9] G. Al-Sayyed, J.C. D'Oliveira, P. Pichat, J. Photochem. Photobiol. A 58 (1991) 99.
[10] A. Mills, S. Morris, R. Davies, J. Photochem. Photobiol. A 70 (1993) 183.
[11] A. Mills, S. Morris, J. Photochem. Photobiol. A 71 (1993) 75.
[12] J. Theurich, M. Lindner, D.W. Bahnemann, Langmuir 12 (1996) 6368.
[13] U. Stafford, K.A. Gray, P.V. Kamat, J. Catal. 167 (1997) 25.
[14] M. Hügül, I. Boz, R. Apak, J. Hazard. Mater. 64 (1999) 313.
[15] L. Palmisano, V. Augugliaro, R. Campostrini, M. Schiavello, J. Catal. 143 (1993) 149.
[16] M.I. Cabrera, A.C. Negro, O.M. Alfano, A.E. Cassano, J. Catal. 172 (1997) 380.
[17] T. Yokota, S. Cesur, H. Suzuki, H. Baba, Y. Takahata, J. Chem. Eng. Jpn. 32 (1999) 314.
[18] M. Salaices, B. Serrano, H.I. de Lasa, Ind. Eng. Chem. Res. 40 (2001) 5455.
[19] D. Curcó, J. Giménez, A. Addardak, S. Cervera-March, S. Esplugas, Catal. Today 76 (2002) 177.
[20] R.J. Brandi, M.A. Citroni, O.M. Alfano, A.E. Cassano, Chem. Eng. Sci. 58 (2003) 979.
[21] Q. Yang, P.L. Ang, M.B. Ray, S.O. Phekonen, Chem. Eng. Sci. 60 (2005) 5255.
[22] B. Toepfer, A. Gora, G. Li Puma, Appl. Catal. B 68 (2006) 171.
[23] S.L. Murov, I. Carmichael, G.L. Hug, Handbook of Photochemistry, second ed., Marcel Dekker, New York, 1993.
[24] M.L. Satuf, R.J. Brandi, A.E. Cassano, O.M. Alfano, Ind. Eng. Chem. Res. 46 (2007) 43.
[25] C. Minero, F. Catozzo, E. Pelizzetti, Langmuir 8 (1992) 481.
[26] E. Pelizzetti, C. Minero, Electrochim. Acta 38 (1993) 47.
[27] C.B. Almquist, P.A. Biswas, Chem. Eng. Sci. 56 (2001) 3421.
[28] G. Palmisano, M. Addamo, V. Augugliaro, T. Caronna, A. Di Paola, E. García López, V. Loddo, G. Marcí, L. Palmisano, M. Schiavello, Catal. Today 122 (2007) 118.
[29] M.F.J. Dijkstra, H.J. Panneman, J.G.M. Winkelman, J.J. Kelly, Chem. Eng. Sci. 57 (2002) 4895.
[30] R. Terzian, N. Serpone, C. Minero, E. Pelizzetti, H. Hidaka, J. Photochem. Photobiol. A 55 (1990) 243.
[31] O.M. Alfano, M.I. Cabrera, A.E. Cassano, J. Catal. 172 (1997) 370.
[32] M.N. Özişik, Radiative Transfer and Interactions with Conduction and Convection, Wiley, New York, 1973.
[33] O.M. Alfano, A.C. Negro, M.I. Cabrera, A.E. Cassano, Ind. Eng. Chem. Res. 34 (1995) 488.
[34] R. Siegel, J.R. Howell, Thermal Radiation Heat Transfer, fourth ed., Hemisphere Publishing Corp., Bristol, PA, 2002.
[35] M.L. Satuf, R.J. Brandi, A.E. Cassano, O.M. Alfano, Ind. Eng. Chem. Res. 44 (2005) 6643.
[36] J.J. Duderstadt, W.R. Martin, Transport Theory, Wiley, New York, 1979 .